UCRL-JC-129725
PREPRINT

Frequency Converter Development for the National Ignition Facility

P. J. Wegner, J. M. Auerbach, C. E. Barker,
S. C. Burkhart, S. A. Couture, J. J. DeYoreo,
R. L. Hibbard, L. W. Liou, M. A. Norton,
P. A. Whitman, L. A. Hackel

This paper was prepared for submittal to the
Third Annual International Conference on
Solid State Lasers for Application (SSLA)
to Inertial Confinement Fusion (ICF)
Monterey, California
June 7-12, 1998

October 30, 1998

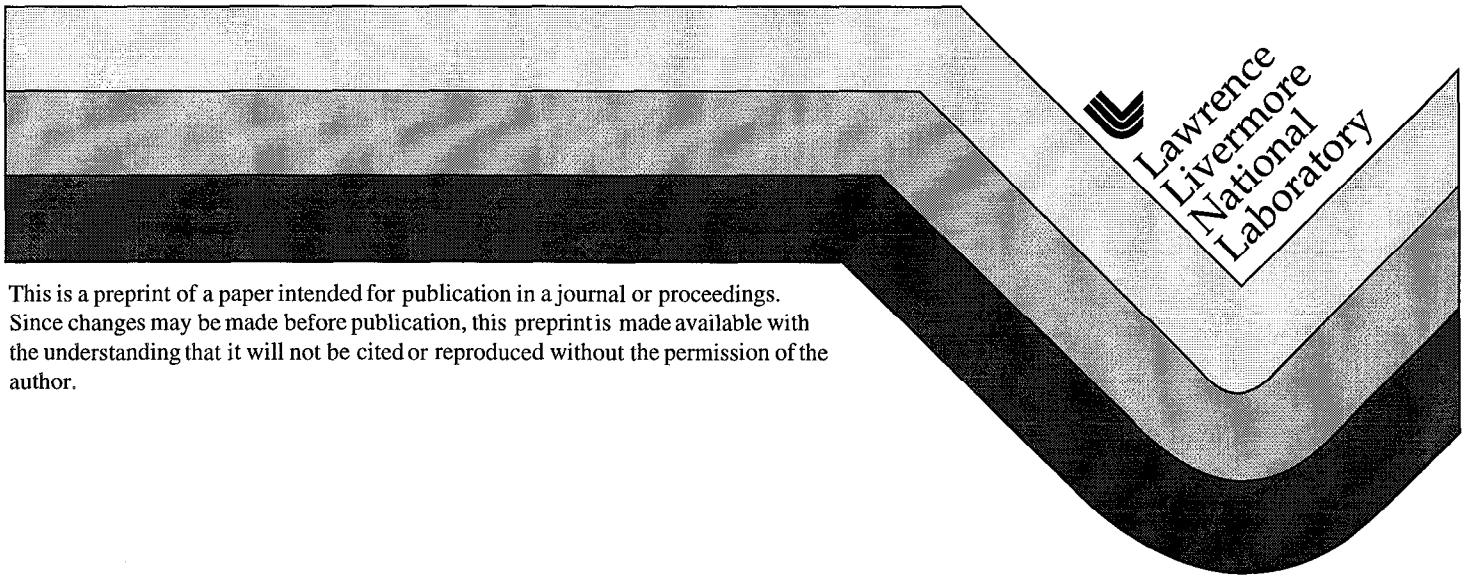

Frequency converter development for the National Ignition Facility

P.J. Wegner, J.M. Auerbach, C.E. Barker, S.C. Burkhart, S.A. Couture, J.J. DeYoreo,
R.L. Hibbard, L.W. Liou, M.A. Norton, P.A. Whitman, L.A. Hackel

University of California, Lawrence Livermore National Laboratory
P.O. Box 808, L-479, Livermore, CA 94550

ABSTRACT

The design of the National Ignition Facility (NIF) incorporates a type I/type II third harmonic generator to convert the 1.053-μm fundamental wavelength of the laser amplifier to a wavelength of 0.351 μm for target irradiation. To understand and control the tolerances in the converter design, we have developed a comprehensive error budget that accounts for effects that are known to influence conversion efficiency, including variations in amplitude and phase of the incident laser pulse, temporal bandwidth of the incident laser pulse, crystal surface figure and bulk non-uniformities, angular alignment errors, Fresnel losses, polarization errors and crystal temperature variations. The error budget provides specifications for the detailed design of the NIF final optics assembly (FOA) and the fabrication of optical components. Validation is accomplished through both modeling and measurement, including full-scale Beamlet tests of a 37-cm aperture frequency converter in a NIF prototype final optics cell. The prototype cell incorporates full-perimeter clamping to support the crystals, and resides in a vacuum environment as per the NIF design.

Keywords: harmonic generation, frequency conversion, nonlinear optics, ICF

1. INTRODUCTION

The wavelength of the NIF Nd:glass amplifier will be converted from 1.053-um (1ω) to 0.351 um (3ω) using cascade type I/type II sum-frequency generation [1]. The basic scheme is diagrammed in Figure 1. Through experiments conducted on the Beamlet prototype laser over the past year, we have gained valuable experience operating and characterizing frequency converters of this type at an aperture-size of 37 cm, and in a prototypical NIF configuration utilizing full-perimeter mounting of the crystals in a compact final optics cell (FOC) in vacuum [2,3]. Based on this experience, we've been able to clearly identify and greatly improve our understanding of the many factors that are expected to impact third-harmonic generation on the NIF. Currently, our level of understanding is such that we've been able to predict 3ω conversion efficiencies on Beamlet to within a few percent of measured values. As a result, it is now clear where we have the greatest leverage for improving performance, and where future engineering efforts must be concentrated.

The close agreement between measurement and theory is the result of well-diagnosed experiments and an accurate physics model, for which the input parameters are firmly grounded on measurements or calculation. The next section briefly reviews this model to summarize the relevant crystal and field parameters that are important for frequency conversion. With the model as a tool we have performed a detailed analysis of the NIF baseline converter design using an error budget approach, in which expected deviations of the relevant parameters from their ideal values constitute "errors" resulting in specific reductions in conversion efficiency. The results of this analysis are compared side by side with the results from an identical analysis applied to a Beamlet converter in Section 3, followed by a more detailed discussion of the Beamlet experimental data that was used to validate the model in Section 4. Section 5 concludes with priorities for future work.

2. FREQUENCY CONVERSION PHYSICS MODEL

The model for the frequency converter is based on the well known coupled amplitude equations for sum-frequency generation in the paraxial slowly-varying envelope approximation [4-6]. In our case the equations include terms for effects we've identified as having small, but non-negligible impacts on frequency conversion: bulk linear loss, diffraction, Poynting vector walk-off, 2-photon absorption at the third harmonic, and nonlinear refractive index. In comparison, the effects of group-velocity dispersion are negligible for our application and are not included in the model.

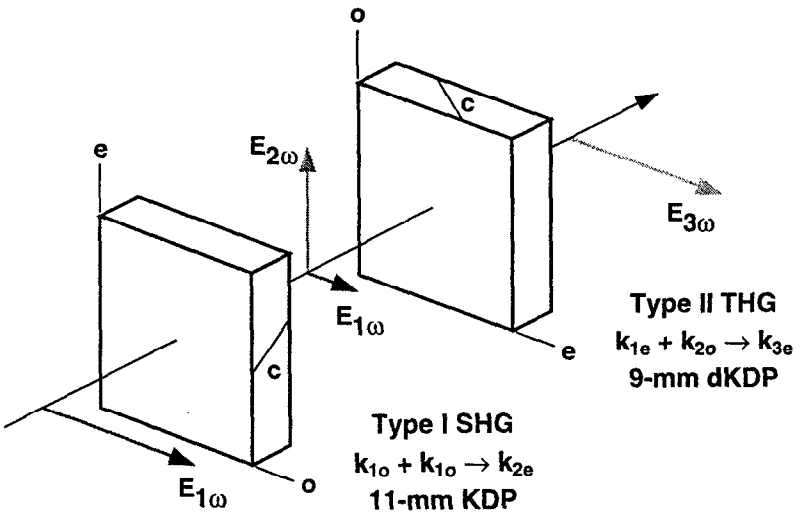

(a)

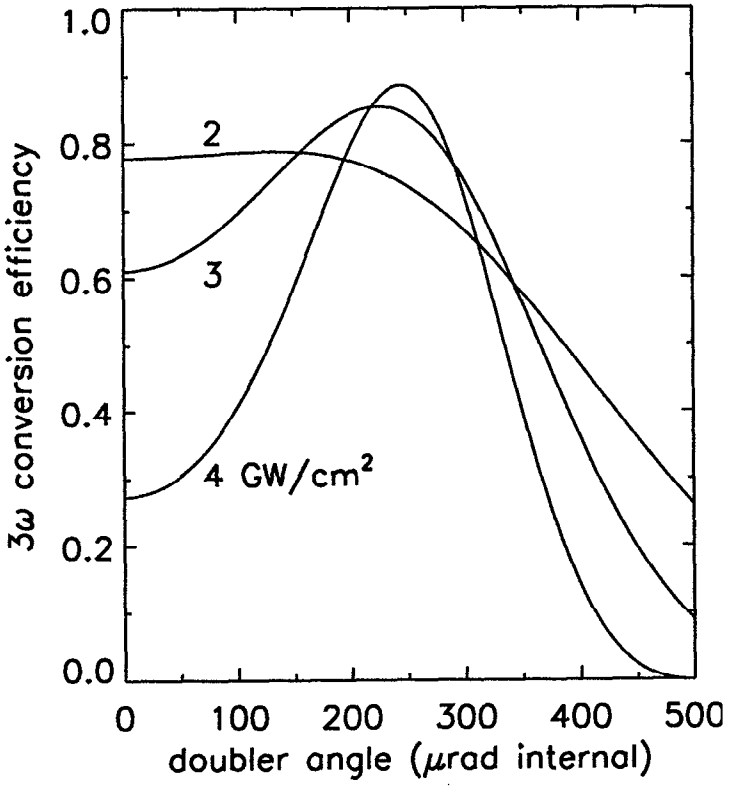

(b)

Figure 1. (a) Frequency conversion scheme for the NIF, consisting of an 11-mm type-I KDP doubling crystal and 9-mm type-II dKDP tripling crystal in series. *c* denotes direction of crystal optic axis. (b) Plane-wave calculation of 3ω conversion efficiency showing how the 1ω/2ω mix ratio for efficient tripling at high irradiance is set by angle-tuning the type-I doubler 200 to 250 μrad from exact phase matching.

With the following definitions for the three fields

$$E_j(x,y,z,t) = \frac{1}{2}\frac{1}{\sqrt{n_j}} A_j(x,y,z,t)\exp[i(k_j z - \omega_j t)] + c.c, \qquad j = 1, 2, 3 \tag{1}$$

the equation for the sum-generated field A_3 has the form

$$\left(\frac{\partial}{\partial z} + \frac{1}{v_{g3}}\frac{\partial}{\partial t}\right)A_3 = -\frac{i}{2k_3}\nabla_\perp^2 A_3 - \frac{1}{2}\left(\alpha_3 + \beta_3\left|A_3\right|^2\right)A_3 + \frac{i}{2}k_{30}\varepsilon_0 c\left(2\gamma_{31}\left|A_1\right|^2 + 2\gamma_{32}\left|A_2\right|^2 + \gamma_{33}\left|A_3\right|^2\right)A_3 - \rho_3\frac{\partial A_3}{\partial r_e} + i\omega_3 K A_1 A_2 \exp[-i\Delta k z] \tag{2}$$

with similar equations applying for A_1 and A_2. In this expression, the quantity having by far the greatest impact on conversion efficiency, and the one that is also the most sensitive to operating conditions, is the momentum mismatch between the three fields

$$\Delta k = k_3 - k_2 - k_1 = \frac{1}{c}[\omega_3 n_3 - \omega_2 n_2 - \omega_1 n_1], \qquad \omega_3 = \omega_1 + \omega_2 \tag{3}$$

which depends critically on the material birefringence (refractive indices n_j), and thus on the frequency of the input fields ω_1, ω_2, the crystal temperature T, and the orientation θ of the crystal optic axis with respect to the field propagation direction. Complicating the picture in large crystals is an effective variation of θ in x and y due to surface refraction and strain effects [7,8]. Some of the strain resides naturally in the crystal as a residue of the growth and fabrication process. In practice, however both θ and T can be treated as applied quantities, extrinsic to the material, and subject to characterization through measurement. For example, errors in average crystal orientation from specified values are either estimated from fabrication tolerances or measured. Variations in θ across the part due to refraction or stress are quantified after mounting using a technique called orthogonal-polarization interferometry, as described in the appendix.

Parameters that are intrinsic to the crystals include the linear and nonlinear loss coefficients α_j and β_j, the nonlinear coefficient for the refractive index γ_{ji}, and the field coupling coefficient

$$K = \frac{d_{eff}}{c\sqrt{n_1 n_2 n_3}} \tag{4}$$

where d_{eff} depends weakly on the orientation as $d_{36}\sin\theta\sin 2\phi$ for type-I, and $d_{36}\sin 2\theta\cos 2\phi$ for type-II. Definition of the losses incurred at each crystal surface and a suitable approximation for the amplitude and phase profiles of the field at the input to the crystals complete the parameter specifications that are required for the model.

3. ERROR ANALYSIS OF FREQUENCY CONVERISON

Using this model we have performed an error analysis of the converter design to determine the performance that can be expected for the NIF ICF mission, and to compare this performance with the peak-power conversion efficiency specified in the current system performance model [9]. In the context of this analysis, factors that cause the parameters of the converter model to deviate from conditions defined as "ideal" constitute "errors" that produce a calculable reduction in conversion efficiency. The effect of each error is calculated separately, and with the assumption that the effects of small

Parameter	units	doubler		tripler*	
l	mm	11.0	[1]	9.0	[1]
α_1	cm^{-1}	0.058	[10]	0.002	[11]
α_2	cm^{-1}	0		0	
α_3	cm^{-1}	0		0	
d_{36}	pm/V	0.39	[10]	0.37	[10,12]
θ_m	degrees	41.2	[13]	60.1	[14]
$\Delta\theta$	μrad	220		0	
surface loss	%	0		0	

* 70% deuteration level

Table I. Parameters of the ideal converter model

errors add independently, we determine both the total reduction in efficiency relative to an ideal converter, and the aspects of the design that are primarily responsible for the loss. The starting point, or zero-error condition which produces maximum achievable tripling efficiency, is a plane-wave flat-in-time input field, an 11-mm thick type-I KDP doubler, and a 9-mm thick type-II dKDP tripler, with both crystals having nominal bulk losses and perfect anti-reflection (AR) coatings. The drive irradiance of 3 GW/cm^2 used in the analysis is slightly higher than the 2.8 GW/cm^2 used in the NIF performance model, as insurance against reductions in the NIF beam size. At 3 GW/cm^2 the optimum tuning for the angle-tuned type-I doubler is 220 μrad (internal) from exact phase matching and the ideal conversion efficiency is 89.4% (see Figure 1). The parameters used in the ideal model are summarized in Table I.

Errors important for the analysis fall into two categories depending on whether they are static or dynamic. Static errors remain invariant from shot to shot and as such, can potentially be compensated for by varying the input 1ω drive irradiance. Errors of this type encompass reductions associated with a non plane-wave 1ω beam, including fill factor, amplitude/phase ripple, depolarization, and bandwidth; linear loss beyond nominal in the crystals and AR coatings; nonlinear loss in the crystals, including 2-photon absorption; and static angular errors in the crystals arising from uncertainties in the optimum tuning angle, or from spatial non-uniformity of the tuning angle associated with crystal quality and mounting distortion. In contrast, dynamic errors vary from shot to shot, cannot readily be compensated, and thus affect our ability to balance power on target. Errors that we've identified of this type can all be related to angle: fluctuations in the crystal temperature, variability in crystal alignment, vibration and drift in the FOA, and pulsed beam pointing errors. The effects of these two categories of errors were evaluated separately.

Current engineering estimates for the dynamic errors are shown in Table II. Because these errors are random they are assumed to root-sum-squares (RSS) add, yielding a total error of ~ ±13 μrad (external angle, 1σ). At 3 GW/cm^2, the angular sensitivity of the type-I doubler is such that a 30-μrad external-angle error varies the conversion efficiency by 1%, and a 55-μrad error varies the efficiency by 3% (the angular sensitivity of the type-II tripler is smaller by a factor of three). The variation in conversion efficiency allowed by the NIF power balance budget is ±1% 1σ, thus the dynamic errors in the FOA should be within this budget.

Error Source	Equivalent $\Delta\theta$ (μrad external, 1σ)	Comments
FOA contributions:		
± 0.1° C short-term thermal drift	± 4	80 μrad (internal) /°C for doubler [15]
Structural motion	± 10 [16]	
FOC alignment	± 2 [17]	most of error is static
Beam contributions:		
pointing jitter	± 7 [17]	
RSS sum	± 13	

Table II. Dynamic error estimates for frequency conversion

Parameter	Ideal value	NIF model value	NIF model Δη (%)	NIF estimate value	NIF estimate Δη(%)	Beamlet value	Beamlet Δη(%)
1ω pulse:							
bandwidth (GHz)	0	30	1.45	30	1.45	30	1.45
depolarization (deg)	0	0	0	3	0.30*	5.4	0.90
spatial fill factor (%)	100	90	0.53	90	0.53	88	
amplitude/phase ripple	0	NIF	0.15	NIF	0.15	Beamlet	1.29
collimation error (λ)	0	0	0	1.25	0.07	0.25	0.1
irradiance (GW/cm^2)	3.0	2.8	0.86	3.0	0	3.0	0
subtotal			2.99		2.22		3.74
Doubler:							
linear loss (%/cm)							
α_{1o}	5.8	5.8	0	5.8	0	5.8	0
α_{2e}	0	0	0	0	0	0	0
surface loss (%)							
R_1 (1ω)	0	0.5	0.56	0.2	0.22	1.65	1.85
R_2 (1ω,2ω)	0	0.5	0.57	0.7	0.80	2.35	2.69
static angle (μrad internal)							
nominal	220	220	0	220	0	220	0
quality/mounting (1σ)	0	0	0	25	1.19	25	1.19
alignment offset	0	0	0	10	0.60*	10	0.60*
thermal correction error	0	0	0	5	0.05*	5	0.05*
subtotal			1.13		2.29		5.76
Tripler:							
linear loss (%/cm)							
α_{1e}	0.2	0.2	0	0.2	0	0.2	0
α_{2o}	0	0	0	0.1	0.03	0.1	0.03
α_{3e}	0	0	0	0.3	0.16	0.3	0.16
nonlinear loss							
$\beta_{3\omega}$ (cm/GW)	0	6.0e-3	0.57	6.0e-3	0.57	6.0e-3	0.57
surface loss (%)							
R_1 (1ω,2ω)	0	0.5	0.57	0.7	0.80	2.35	2.69
R_2 (3ω)	0	0.5	0.50	0.2	0.20	1.30	1.30
static angle (μrad internal)							
nominal	0	30	0.28	0	0	0	0
quality/mounting (1σ)	0	0	0	75	1.86	75	1.86
alignment offset	0	0	0	10	0.09*	10	0.09*
thermal correction error	0	0	0	20	0.12*	20	0.12*
subtotal			1.92		3.62		6.61
Net efficiency (%)	89.4	84.1		82.3		75.8	

Table III. Static error estimates for frequency conversion

The individual and cumulative effects of the static errors are summarized in Table III, which lists the representative values for the parameters in the model and their calculated effect on the efficiency for three cases: the converter in the system performance model, a converter based on current NIF engineering estimates, and a converter as tested on Beamlet. Entries in the table are grouped according to whether they are associated with the input field, the doubler, or the tripler. To calculate the total losses in performance listed at the bottom of the table, the absolute percent losses in each of the three groups were added together, divided by 100, and subtracted from one to generate three separate

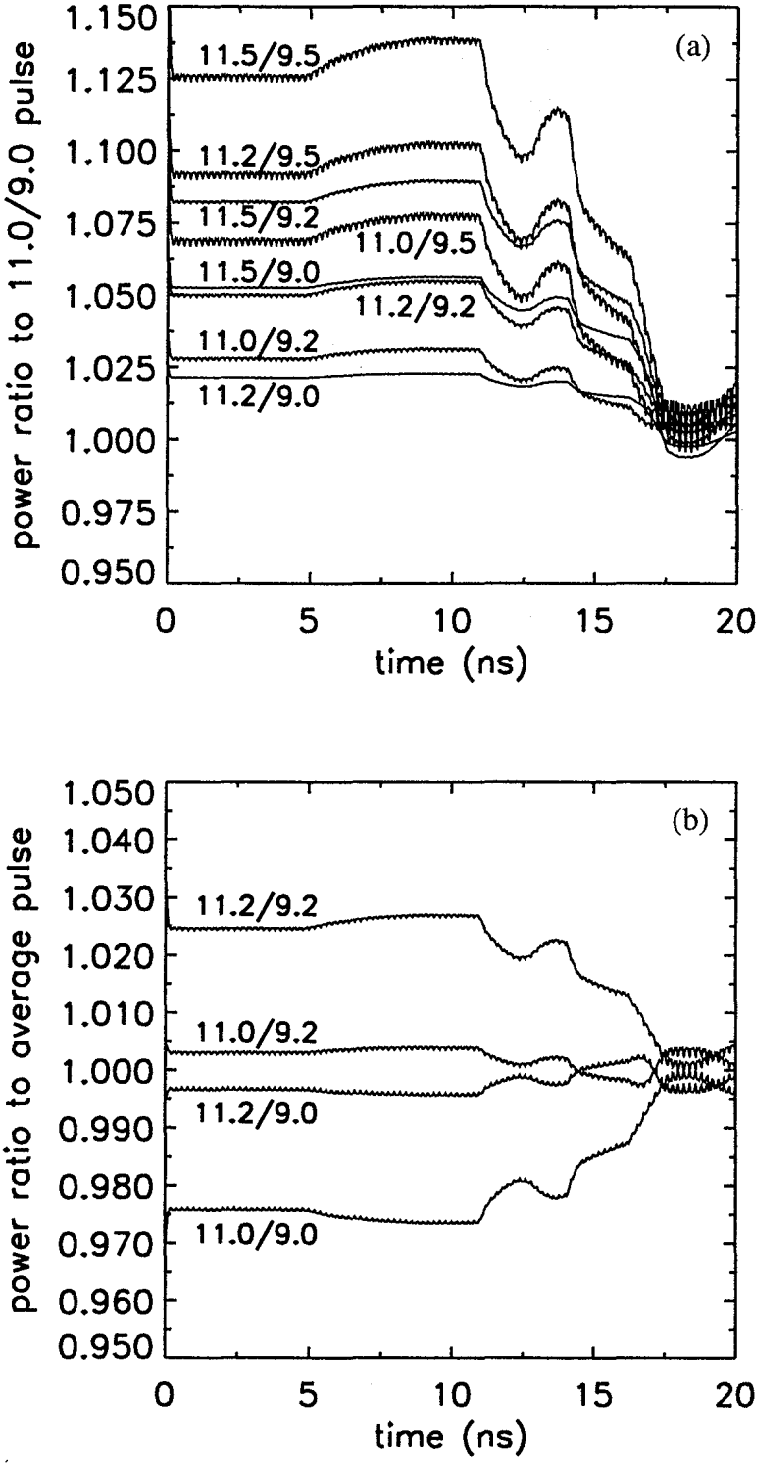

Figure 2. (a) Calculation of 3ω power versus time in the 20-ns shaped ICF ignition pulse for various crystal thicknesses, normalized to the 3ω power produced by the baseline 11.0-mm doubler//9.0-mm tripler combination. (b) Similar plot for four crystal thickness combinations representing limits of the current 2-mm tolerance, normalized to the average power produced by the four combinations. High-frequency structure is the result of the applied 30-GHz SBS-suppression bandwidth.

derate factors for the ideal efficiency. Losses denoted by an asterisk represent 1σ values for an expected distribution and were RSS added. The efficiencies in the table were calculated for flat-in-time pulse shapes, and as such correspond to aperture-averaged peak-power conversion efficiencies at 3 GW/cm^2. A less-than-unity temporal fill factor such as that of a real pulse will further decrease the efficiency.

Examining the table we find that the 84.1% efficiency for the NIF model case is within 0.6% of the value in the current NIF system performance model, lending confidence that the error-analysis approach is sound. The conversion efficiency based on current NIF engineering estimates is a few percent lower than that in the system model, primarily due to angular errors not included in that model. On the other hand, the NIF estimate is over 6% higher than the conversion efficiency predicted for the rapid-growth Beamlet converter described in the next section. Only a small part of the discrepancy between the NIF and Beamlet result is related to differences between the NIF and Beamlet beams. The majority is associated with surface losses caused by rapid degradation of the sol-gel anti-reflection coatings in the vacuum test environment, that are currently not in the NIF engineering estimate. As a result, coatings are an area of uncertainty in this design and have a high priority for future development efforts. In addition, two other aspects of the design require attention to ensure that the specifications reflected in the budget are carried successfully to the NIF. First, the tight angular tolerances of the converter are such that the tripler must phase match at angle of 10.58 mrad ± 30 μrad (external) relative to the beam direction, as fixed by the NIF system design. The fabrication and metrology process to meet this tolerance requires some additional development and testing, including the design and implementation of a machine to correctly orient the crystal surfaces during fabrication, and the development of a means to verify the optimum tilt angle for the assembled FOC to within the 10 μrad specified in the static error budget, prior to installation on the NIF. Both of these efforts are currently underway. Second, the tolerance for long-term temperature drift in the FOA is ±0.3 °C, which is large enough that some amount of compensating adjustments to the tilt angle of the FOC will be required. Fully compensating the tripler, which thermally tunes at a rate of ~200 μrad/°C, is expected to use up approximately two-thirds of the alignment and diagnostics sensor's field of view.

Crystal thickness is a special case of a static error that directly impacts power balance. As shown in Figure 2, the conversion efficiency is most sensitive to crystal thickness in the low-irradiance foot of the shaped ICF ignition pulse. The current specified tolerance of 0.2 mm meets the budgeted allocation for power balance throughout the pulse (Figure 2b) and allows the crystals to be refinished at least once. Fortunately, crystal thickness variations can be budgeted independently of the dynamic errors in Table II, since the angular errors in Table II affect power balance only at high irradiance, where sensitivity to angle is large, but sensitivity to crystal thickness is small.

4. BEAMLET

The model used in the error analysis has been tested and validated over the course of several frequency conversion experimental campaigns conducted on Beamlet. Extensive diagnostics provided an accurate and complete set of input parameters for the model, as well as the frequency conversion performance data to which it was compared. Off-line diagnostics included orthogonal-polarization interferometry to determine crystal refractive index non-uniformities, and photometry to measure crystal surface losses and bulk transmission, both before and after the experiments. On-line diagnostics included calorimetry to measure the input and output pulse energies, scientific-grade CCD cameras to record the input and output near-field fluence distributions, and streak cameras to record the input and output temporal pulse shapes. Several Beamlet test configurations, summarized in Table IV, were used to evaluate both second-harmonic generation (SHG) and third-harmonic generation (THG) with converters consisting of both conventionally-grown and rapidly-grown crystals [18]. All of the crystals were mounted in a prototype 37-cm aperture FOC and tested in the vacuum environment of the FOA test mule [19,20]. The configuration of the Beamlet amplifier was the same for all tests: eleven cavity amplifiers, five booster amplifiers, a 200-μrad carbon pinhole in the pass-4 cavity spatial filter pinhole, and a 150-μrad stainless-steel cone pinhole in the transport filter. Pulse format was 1.5-ns square. Estimated accuracy of the conversion efficiency measurements was ± 6% (3σ).

SHG efficiencies measured with a conventionally-grown type-I doubler from a NIF production boule are plotted in Figure 3(a). Maximum energy efficiency was 73% (aperture averaged, time integrated) at an input 1ω irradiance of

Parameter	Conventional growth		Rapid growth	
	SHG	THG	SHG	THG
1ω laser				
beam size (cm)	34	34	34	30
Doubler				
serial number	345-1	345-1	RG8B-2	RG8B-2
thickness (mm)	11.09	11.09	11.10	11.10
Δθ distribution (μrad int, 1σ)	22.3	18.8	17.5	27.8
surface loss (% before/after)				
S_1 (1ω)	0.91/ -	- /1.49	1.03/ -	1.64/1.67
S_2 (1ω)	0.91/ -	- /1.49	1.03 -	1.64/1.67
S_2 (2ω)	1.70/ -	- /2.53	1.48/ -	2.85/3.30
Tripler				
serial number	-	LL1-37-1	-	RG8A-1
thickness (mm)	-	9.48	-	9.41
deuteration level (%)	-	70	-	85
Δθ distribution (μrad int, 1σ)	-	36.2	-	67.7
surface loss (% before/after)	-		-	
S_1 (1ω)	-	0.60/ -	-	2.75/3.05
S_1 (2ω)	-	1.82/ -	-	1.30/2.20
S_2 (3ω)	-	0.10/ -	-	0.37/2.21
Measured performance				
maximum energy efficiency (%)	73	75	70.5	73.5
at 1ω irradiance (GW/cm^2)	4.0	3.8	3.9	3.6

Table IV. Configuration and results summary for Beamlet
FOA test mule frequency conversion experiments

approximately 4 GW/cm^2 (aperture averaged, peak in time). Similar tests of a rapidly-grown type-I doubler achieved 70.5% efficiency at similar drive irradiance. The measured performance of these crystals was in good agreement with modeling based on measured 1ω pulse parameters and measured crystal refractive-index variations. The effects of the latter were enhanced by measuring the 2ω near-field fluence distributions with the crystal tilt biased well away from exact phase matching. As shown in Figure 4, the resulting non-uniformities in the data were well-reproduced in the model.

THG efficiencies measured with a rapidly-grown doubler and tripler are plotted in Figure 3(b). Maximum energy efficiency was 73.5% at an input 1ω irradiance of approximately 3.6 GW/cm^2. In comparison the model, with an input field based on near-field 1ω irradiance data and an eleven time-slice approximation of the measured 1ω pulse shape, predicted an energy conversion efficiency of 77%, and a peak-power conversion efficiency of 79.5%. Correcting the model to account for the 30-GHz bandwidth of the drive pulse, and the measured depolarization in the Beamlet laser (see Table III), lowers the calculated energy efficiency to 75%. Incorporating the additional losses caused by the degradation of the sol-gel AR coatings over the course of the experiment further reduces the efficiency to 71.5%, suggesting that the model is accurate to within the uncertainty in the component transmissions (the calculated peak-power conversion efficiency in this case is 74%). Calculated and measured near-field fluence distributions for both the third harmonic and residual second-harmonic fields shown in Figure 5 are in fairly good agreement as a result of having the orthogonal-polarization interferomery data incorporated in the model. The energy balance in the model (the ratio of total energy out of the converter to total energy into the converter) is ~3% higher than observed, consistent with the actual transmissions of the components in vacuum being lower than the initial values modeled.

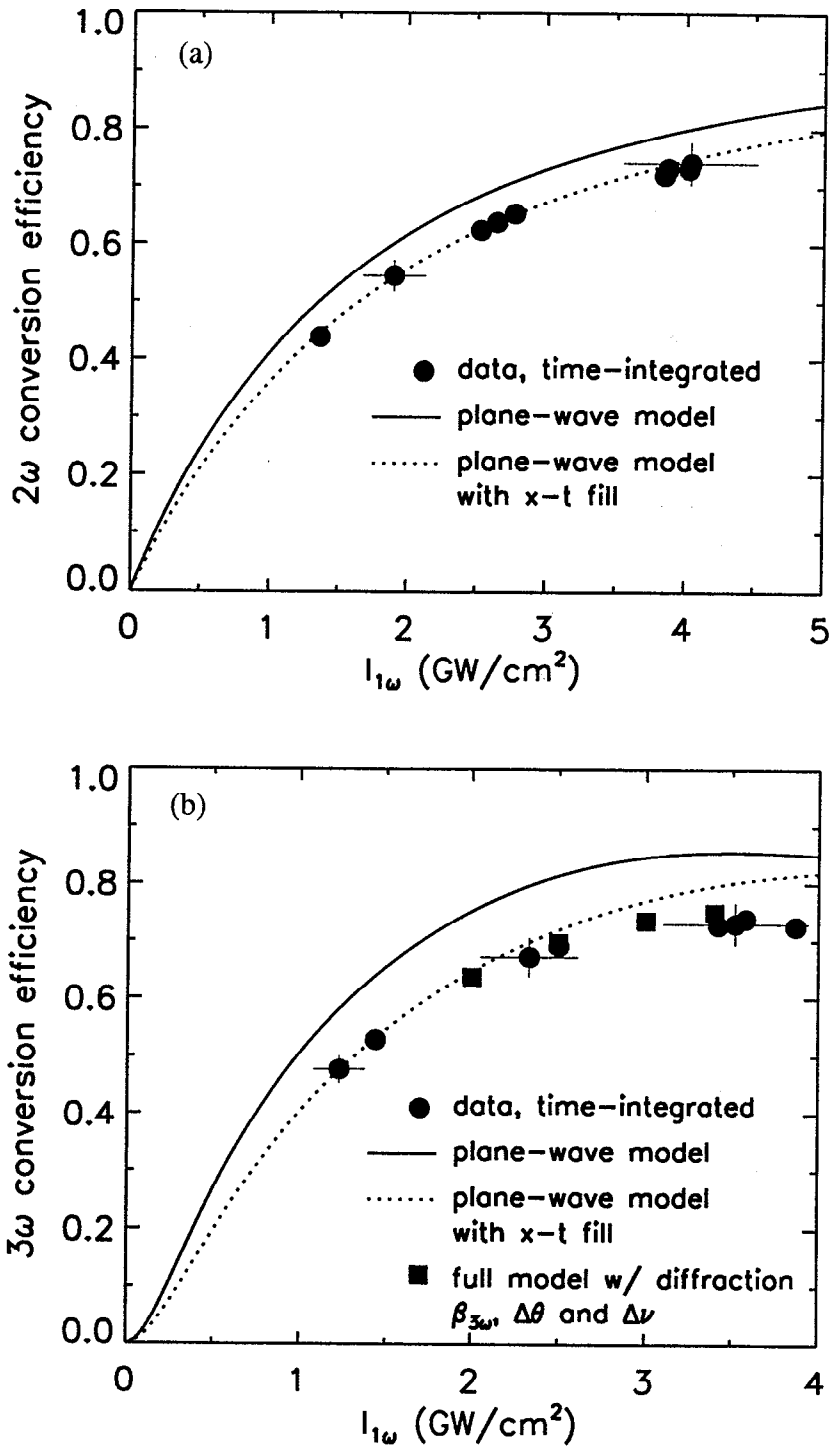

Figure 3. (a) Plot comparing measured and calculated SHG efficiency versus 1ω irradiance for conventional-growth doubler 345-1. (b) Comparison of measured and calculated THG efficiency for rapid-growth doubler RG8B-2 and tripler RG8A-1.

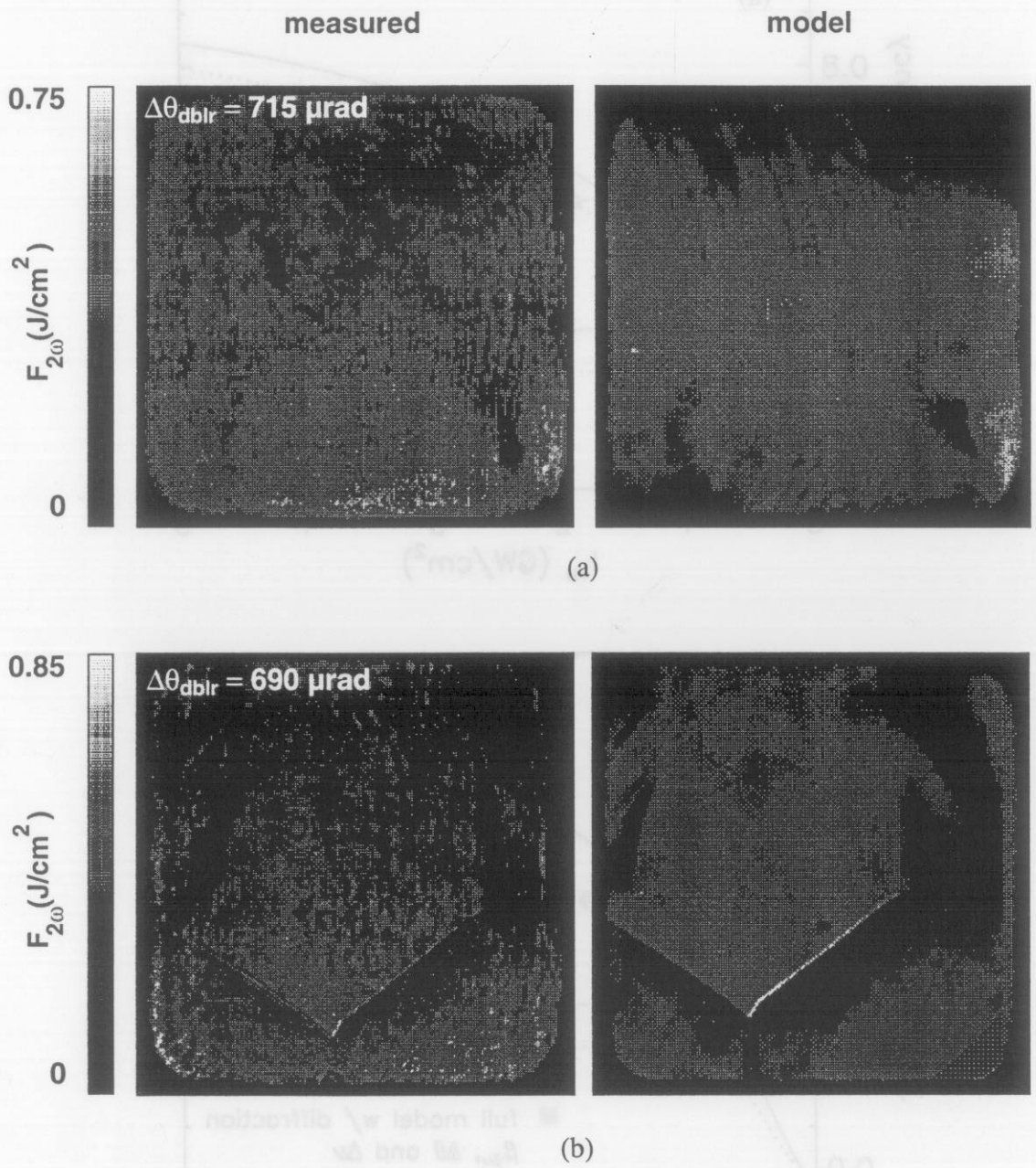

Figure 4. (a) Comparison of measured and modeled 2ω near-field distributions for conventional-growth doubler 345-1. Drive irradiance was 3.9 GW/cm^2. Measured and modeled conversion efficiencies were 6.7 and 6.5% respectively at an angular detuning of 715 µrad (internal). (b) Similar comparison for the rapid-growth doubler RG8B-2. Drive irradiance was 4.2 GW/cm^2. Measured and modeled conversion efficiencies were 6.6 and 7.0% respectively at an angular detuning of 690 µrad (internal). Sharp features in (b) are the boundaries between {101} (pyramidal) and {100} (prismatic) growth regions in the crystal. Conventional growth material is all pyramidal.

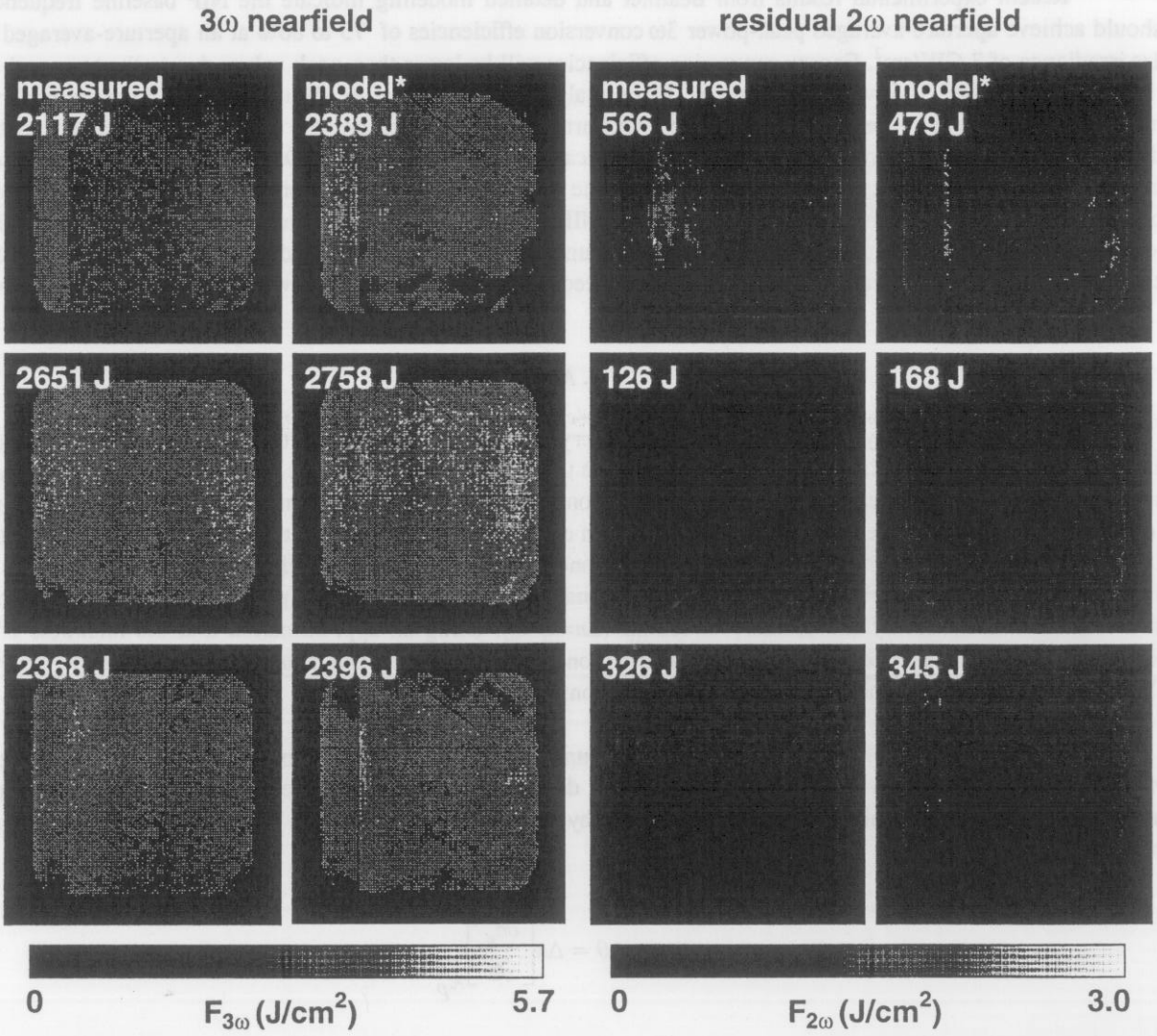

Figure 5. Comparison of measured and modeled near-field fluence distributions for the rapid-growth converter on three different shots in which the tripler angle was varied while the doubler angle was held fixed at 220 μrad. Drive irradiance was 3.4 ± 0.05 GW/cm^2. Measured 3ω conversion efficiencies top to bottom were 56, 73 and 66%,

5. CONCLUSION

Recent experimental results from Beamlet and detailed modeling indicate the NIF baseline frequency converter should achieve aperture-averaged peak-power 3ω conversion efficiencies of 75 to 80% at an aperture-averaged peak-power 1ω irradiance of 3 GW/cm^2. Energy conversion efficiencies will be lower than peak values due to the temporal fill-factor of the drive pulse which is always less than one. Error analysis has been used to identify aspects of the converter design that have high leverage for improving performance. Of particular importance are the sol-gel anti-reflection coatings, which degrade rapidly to a few percent loss per surface in typical vacuum environments. Of lesser concern, but representing some uncertainty, are the tight angular tolerances to which the crystals must be cut and oriented in the final optics cell to ensure phase-matching within the narrow field of view of the NIF output sensor, and the relatively loose tolerance of ±0.3°C for the long-term thermal stability of the FOA, which will require compensating angular adjustments to the FOCs with associated errors. Further attention in each of these areas will be needed to ensure 80% peak-power conversion efficiency on NIF.

6. APPENDIX

Each converter crystal has two orthogonal crystal axes of interest in the plane normal to the direction of propagation, denoted as ordinary and extraordinary. The three fields in the harmonic conversion process are polarized along one or the other of these axes. In orthogonal- polarization interferometry , two transmission interferograms are made of the crystal with linearly-polarized light of wavelength λ_p; in one interferogram, the light polarization is parallel to the ordinary axis; in the second interferogram, the light polarization is parallel to the extraordinary axis. The difference of the two interferograms gives a distribution which is proportional to the thickness of the part times the difference of refractive indices in the extraordinary and ordinary directions ($\Delta n = n_e - n_o$). Using an approximation that the thickness of the part is constant we extract an approximate spatial Δn distribution from the data that can be used to model local departures from the phase-matching condition and thus predict local reductions in conversion efficiency.

Figure 6(a) shows histograms of representative Δn distributions obtained from orthogonal-polarization interferograms of both conventional and rapid-growth doublers and triplers, expressed in terms of equivalent detuning angles. The equivalent detuning angles were calculated by assigning the variations in Δn to local changes in the direction of the crystal optic axis, so that

$$\Delta\theta = \Delta n \left[\frac{\partial n_e}{\partial \theta} \right]^{-1}_{\lambda_p} \tag{A1}$$

The relative impacts of these angular distributions on 3ω conversion efficiency have been calculated separately using the plane wave model, and are plotted versus drive irradiance in Figure 6(b). The results predict the conversion efficiency at 3.5 GW/cm^2 for a converter using rapid-growth crystals to be 2% lower than one using conventional-growth crystals, in nominal agreement with the 1.5% measured on Beamlet and the 2.5% predicted by a full-diffraction calculation.

7. ACKNOWLEDGMENTS

We would like to thank John R. Murray for his significant contributions to the formulation of the frequency conversion error budget. Susan N. Locke helped with the procurement of the Beamlet test crystals. The crystals were machined at Cleveland Crystals Inc. Processing and assembly took place at LLNL under a team led by Michael E. Werve and Terry D. Schwinn. Special thanks to Tim L. Weiland and the Beamlet operations team for their invaluable support in conducting the experiments.

*This work was performed under the auspices of the U.S. Department of Energy by Lawrence Livermore National Laboratory under contract No. W-7405-Eng-48.

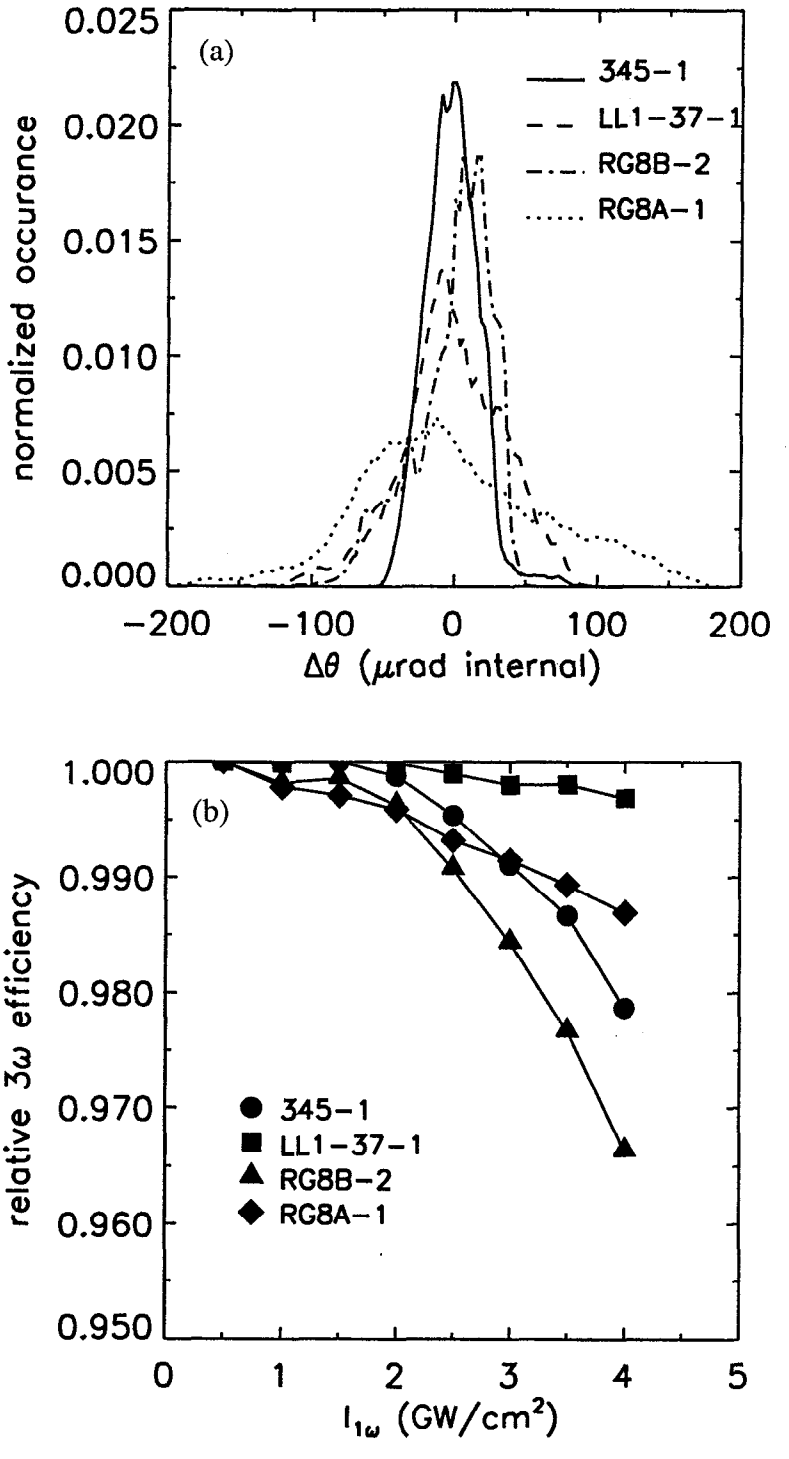

Figure 6. (a) Distribution of phase-match angles in the test crystals inferred from orthogonal-polarization interferometry (b) Plane-wave calculation showing the effect of the individual distributions on 3ω conversion efficiency versus 1ω irradiance. Nominal detuning angles for the doublers and triplers were 220 and 0 μrad respectively.

8. REFERENCES

1. C.E. Barker, B. M. VanWonterghem, J.M. Auerbach, R.J. Foley, J.R. Murray, J.H. Campbell, J.A. Caird, D.R. Speck, and B. Woods, "Design and performance of the Beamlet laser third harmonic frequency converter," *Proc. Soc. Photo-Opt. Instrum. Eng.*, Vol. 2633, 398 (1995).
2. R.E. English Jr.,J. Miller, C. Laumann, and L. Seppala, *ICF Annual Report*, Lawrence Livermore National Laboratory, Livermore, CA, UCRL-LR-105821-97, 112 (1997).
3. V. Karpenko, C. Adams, J. Chael, P. Dohoney, R. Foley, W. Gibson, W. Hibbard, W. Horton, J. Latkowski, D. Lee, A. McDonald, W. Miller, W. Olson, L. Parietti, C. Patel, L. Pittenger, P. Pittman, T. Reitz, D. Trummer, H. Walther, R. Wavrik, W. Weed, and K. Wong, *ICF Annual Report*, Lawrence Livermore National Laboratory, Livermore, CA, UCRL-LR-105821-97, 166 (1997).
4. J.A. Armstrong, N. Bloembergen, J. Ducuing, and P.S Pershan, "Interactions between light waves in a nonlinear dielectric," *Phys. Rev.*, Vol. 127, 1918 (1962).
5. D. Eimerl, J. M Auerbach, and P.W. Milonni, "Paraxial wave theory of second and third harmonic generation in uniaxial crystals. I. Narrowband pump fields," *J. Mod. Opt.*, Vol 42, 1037 (1995).
6. J.M. Auerbach, C.E. Barker, D. Eimerl, K.R. Manes, D. Milam, P.W. Milonni, J.B. Trenholme, and B. VanWonterghem, *ICF Quarterly Report*, Lawrence Livermore National Laboratory, Livermore, CA, UCRL-LR-105821-96-4, 199 (1996).
7. J.J. DeYoreo and B. Woods, "A study of residual stress and the stress-optic effect in mixed crystals of $K(D_xH_{1-x})_2P\ O_4$," *J. Appl. Phys.*, Vol. 73, 7780 (1993).
8. J.M. Auerbach, C.E. Barker, S.A. Couture, D. Eimerl, J.J. DeYoreo, R.L. Hibbard, L.W. Liou, M.A. Norton, S.A. Perfect, P.J. Wegner, and L.A. Hackel, "Modeling of frequency doubling and tripling with converter crystal refractive index spatial non-uniformities," Third International Conference on Solid-State Lasers for Application to Inertial Confinement Fusion, Monterey, CA., June 10, 1998.
9. R. Sacks and W. Williams, "NIF performance summary for the 11-0-5 configuration," internal report NIF-000858, Lawrence Livermore National Laboratory, Livermore, CA. 94550 (1996).
10. D. Eimerl, "Electro-optic, linear, and nonlinear optical properties of KDP and its isomorphs," *Ferroelectrics*, Vol. 72, 95 (1987).
11. C.A. Ebbers, J. Happe, N. Nielsen, and S.P. Velsko, "Optical absorption at 1.06 μm in highy deuterated potassium dihydrogen phosphate," *Appl. Opt.*, Vol. 31, 1960 (1992).
12. V.G. Dmitriev, G.G. Gurzadyan, and D.N. Nikogosyan, *Handbook of Nonlinear Crystals*, Springer-Verlag, Berlin, 1991.
13. Calculated from the refractive index data of Zernike in Ref. 9.
14. Calculated from refractive index data of Kirby in Ref. 9 and extrapolated to 70% deuteration.
15. R.S. Craxton, S.D. Jacobs, J.E. Rizzo, and R. Boni, "Basic properties of KDP related to the frequency conversion of 1-μm laser radiation," *IEEE J. Quant. Elec.*, Vol. QE-17, 1782 (1981).
16. C. Adams, "Angular thermo-mechanical stability budget for the NIF frequency conversion crystals," internal report NIF-0002724-0B, Lawrence Livermore National Laboratory, Livermore, CA. 94550 (1997).
17. E. Bliss, "NIF alignment system accuracy for frequency conversion crystals," internal report NIF-0008425, Lawrence Livermore National Laboratory, Livermore, CA. 94550 (1997).
18. N.P. Zaitseva, J.J. De Yoreo, M.R. DeHaven, R.L. Vital, K.E. Montgomery, M. Richardson, and L.J. Atherton, "Rapid growth of large-scale (40-55 cm) KH_2PO_4 crystals," *J. Cryst. Growth*, Vol. 180, 255 (1997).
19. P.J. Wegner, J.M. Auerbach, C.E. Barker, K.R. Brading, J.A. Britten, S.C. Burkhart, J.A. Caird, S.N. Dixit, P. Feru, M.A. Henesian, R.L. Hibbard, M.R. Kozlowski, D. Milam, J.E. Murray, M.A. Norton, J.E. Rothenberg, T.L. Weiland, W.H. Williams, S.E. Winters, B.M. VanWonterghem, and R.A. Zacharias, "Recent performance results of the Beamlet prototype for the National Ignition Facility," Conference on Lasers and Electro-Optics, San Francisco, CA., May 7, 1998
20. S.C. Burkhart, K.R. Brading, P.M. Feru, M.R. Kozlowski, J.E. Murray, J.E. Rothenberg, B.M. VanWonterghem, P.J. Wegner, and T.L. Weiland, "High-fluence and high-power 1.05-μm ad 351 nm performance experiments on Beamlet," Third International Conference on Solid-State Lasers for Application to Inertial Confinement Fusion, Monterey, CA., June 9, 1998.